Progress In Electromagnetics Research, PIER 75, 329–356, 2007

A NEW METHOD FOR CLASSIFICATION AND IDENTIFICATION OF COMPLEX FIBER BRAGG GRATING USING THE GENETIC ALGORITHM

A. Rostami and A. Yazdanpanah-Goharrizi

Photonics and Nanocrystals Research Lab. (PNRL)
Faculty of Electrical and Computer Engineering
University of Tabriz
Tabriz 51664, Iran

Abstract—In this paper a novel intelligent method to identify an unknown medium (type of apodization and chirping) is developed. Our consideration is concentrated on complex fiber Bragg Gratings. For realization of the idea the Genetic Algorithms (GAs) is used. So, GAs is used to solve inverse scattering problem for reconstruction of nonuniform or complex fiber Brag gratings. In this method, the reflection coefficient measured in practice is inserted to a suitable algorithm. According to the proposed method, first medium discrimination is performed between predefined large classes of mediums and then the whole and necessary parameters for reconstruction of the medium are extracted. Full numerical method is used for compare of the results obtained from the presented algorithm. Our simulation shows good agreement between them. So, a novel method for identification and discrimination of optical mediums especially complex Bragg Gratings is presented. Finally the presented method can be used to identify optical mediums and complex Bragg Gratings systems.

1. INTRODUCTION

The problem of synthesizing or reconstructing a nonuniform fiber Bragg gratings (FBG) and complex structures from its corresponding reflection response is extremely important and efficient in practice for introducing efficient design rules. Usually, in optical communication systems and devices the complex Bragg Gratings including chirped, Apodized and simultaneously chirped and apodized cases are used and these elements have critical applications. For example optical

filters used in dense wavelength division multiplexing (DWDM) system, multiplexing/demultiplexing (MUX/Demux) and many other interesting applications are realized by these devices. Optical sensors such as temperature, ultrasound signal detection, pressure detectors and many other sensory applications need complex Bragg Gratings. Also, these structures have important role in stable single mode and single frequency laser design [1–5]. Several experimental techniques have been demonstrated to fabricate nonuniform gratings, permitting an accurate control of both the local grating pitch and the apodization profile along the structure [6, 7]. These techniques give substantial flexibility to the grating design process. For presentation of high quality devices and systems, identification of implemented elements is critical, which in these cases the inverse problem should be solved.

Inverse scattering techniques [8] offer a great variety of possibilities for the design of gratings. For weak gratings, the synthesis problem of fiber gratings reduces to an inverse Fourier transform of the reflection coefficient. This is known as the first-order Born-approximation, and applies only for gratings including small reflectivity. Several modifications made for improving the method to consider high reflectivity [9, 10]. For example the Fourier transform technique has been extended by Winick and Roman [4] yielding a better approximation and enabling the design of practical fiber grating filters. However, this synthesis procedure is approximate in nature and, consequently, not reliable for the design of very complex filters.

An exact solution of this inverse scattering problem was found by Song and shin [8] and they solved the coupled Gel'fand-Levitan-Marchenko (GLM) integral equations that appear in quantum mechanics. Their method is exact, but it is restricted to the reflection coefficient that can be expressed as a rational function. However, approximating the desired spectral response by rational functions is difficult (generally) and also can give some inaccuracies. To overcome this limitation, an iterative solution of the Gel'fand-Levitan-Marchenko (GLM) system was proposed by Peral to synthesize arbitrary spectral responses [2, 11]. Some fiber grating designs calculated with this method have already been fabricated, proving the usefulness of the method [12]. The iterative solution of the GLM equations [13] has some weaknesses.

However, the solution is approximate due to the finite number of iterations computed, which translates into considering only a limited number of reflections within the medium. This is particularly noticeable for strong gratings with discontinuities in the coupling function. Also, when specifying ideal filter responses, it is desirable to have a weighting mechanism, which makes it easier to weight the

different requirements. The iterative GLM method does not support such a mechanism in a satisfactory way.

Another group of exact inverse scattering algorithms called differential or direct methods [14–17]. These techniques, developed by geophysicists like Robinson and Goupillaud [14, 15], exploit fully the physical properties and structure of the layered media in which the waves propagates. The methods are based again on causality arguments and identify the medium recursively layer by layer. For this reason, they are sometimes called layer-peeling or dynamic deconvolution algorithms.

Also, there are some other published papers which were discussed about different aspects of Bragg Gratings [18–27].

Recently, several heuristic approaches have been developed for the solution of the inverse problem with the goal of designing gratings as filters for telecommunication applications. Skaar, Risvik and Cormier et al. developed genetic algorithms (GA) for extraction of the physical parameters of the Bragg gratings from the measured reflected intensity spectrum [28, 29]. Skaar and Risvik encoded the grating coupling coefficient using a real number formulation and they applied the Runge-Kutta algorithm to calculate the spectral response of the grating [28]. Cormier et al. instead reduced the spectral response calculation time using the Transfer Matrix (T-matrix) formulation [29]. This formulation is based on approximating the coupling coefficients of grating as a piecewise constant function along the grating. Cormier et al. characterized the Bragg gratings in terms of three distinguishable parameters such as the Grating length, period and amplitude of the modulated index of refraction [29].

In all previous works the apodization functions of the gratings are assumed to be known before reconstruction but in this paper we demonstrate a new technique for discrimination of the kind of apodization or chirp function and then the identification of the parameters is done. Our algorithm is based on GAs. First medium discrimination is performed between a large classes of predefine types and then using GAs medium parameters are extracted precisely. Genetic algorithm was applied to similar electromagnetic problems too [30–34].

The organization of the paper is as follows.

In Section 2 the mathematical background for modeling of the complex Fiber Bragg Grating is presented. Also, in this section the Transfer Matrix method is discussed. The genetic algorithm and it application to inverse problem is investigated in Section 3. The simulation results and discussion will be presented in Section 4. Finally the paper ends with a conclusion.

2. MATHEMATICAL FORMALISM FOR MODELING OF FIBER BRAGG GRATING

A fiber Bragg grating is a periodic perturbation structure of the refractive index in a waveguide. The Apodized and chirped index of refraction for the fiber Bragg gratings can be written as follows [35].

$$n(x,y,z) = n_0 + \delta n_0 + g(z)\delta n(z)\cos\left[\frac{2\pi}{\Lambda}z + \Phi(z)\right], \qquad (1)$$

where the average refractive index $\overline{n}$ is represented as $n_0 + \delta n_0$ and $n_0 \geq \delta n_0$. In Eq. (1) $n_0, \delta n_0, \delta n(z), \Phi(z), \Lambda, g(z)$ are the refractive index of the core without perturbation, the average index modulation (DC change), the small amplitude of the index modulation, the position dependent phase of the grating, the Bragg period and the apodization function respectively.

In most fiber gratings, the induced index change is approximately uniform across the core, and there are no propagation modes outside the core of the fiber. In terms of this supposition, the cladding modes in the fiber are neglected in this paper. If we neglect the cladding modes, the electric field of the grating can be simplified only to the superposition of the forward and backward fundamental mode in the core. The electric field distribution along the core of the fiber can be expressed in terms of two counter-propagating modes under the two-mode approximation [36].

$$E(x,y,z) = [A^+(z)\exp(-i\beta z) + A^-(z)\exp(i\beta z)]e_t(x,y) \qquad (2)$$

where $A^+(z)$ and $A^-(z)$ are slowly varying amplitudes of the forward and backward traveling waves along the core of the fiber respectively. The $E(x,y,z)$ can be substituted into coupled-mode equations [37]. The coupled-mode equations can be simplified into two modes, which are described as

$$\begin{aligned} \frac{dR(z)}{dz} &= i\hat{\sigma}(z)R(z) + ik(z)S(z) \\ \frac{dS(z)}{dz} &= -i\hat{\sigma}(z)R(z) - ik^*(z)R(z) \end{aligned}, \qquad (3)$$

where $R(z)$ and $S(z)$ are the forward and backward modes respectively and they represent slowly varying mode envelope functions. The $\hat{\sigma}$ and $k(z)$ are self-coupling coefficient [37] that is called local detuning and the ac coupling coefficient [37] (called local grating strength [38]) respectively.

The simplified coupled-mode equation (Eq. (3)) is used in the simulation of the spectral response of the Bragg grating. The coupling

coefficient $k(z)$ and the local detuning $\hat{\sigma}$ are two important parameters in the couple-mode equations (3). They are fundamental parameters in the calculation of the spectral response of the fiber Bragg gratings. The notations of these two parameters are different, depending on the different authors in literature.

The general self-coupling coefficient can be represented by

$$\hat{\sigma} = \delta + \sigma - \frac{1}{2}\frac{d\Phi}{dz}, \tag{4}$$

where $\frac{d\Phi}{dz}$ is describes possible chirp of the grating period [37]. The detuning δ can be represented by

$$\delta = \beta - \frac{\pi}{\Lambda} = \beta - \beta_D = 2\pi n_{eff}\left(\frac{1}{\lambda} - \frac{1}{\lambda_D}\right), \tag{5}$$

where $\lambda_D = 2n_{eff}\Lambda$ is the design wavelength for Bragg reflectance.

$$\sigma = \frac{2\pi}{\lambda}\overline{\delta}n_{eff}, \tag{6}$$

where $\overline{\delta}n_{eff}$ is the background refractive index change. The coupling coefficient can be represented by

$$k(z) = \frac{\pi}{\lambda}\delta n(z)g(z). \tag{7}$$

The coupling coefficient is proportional to the modulation depth of the refractive index $\Delta n(z) = \delta n(z)g(z)$.

For obtaining the reflection coefficient of a fiber Bragg grating we used the transfer matrix method as follows. The transfer matrix method can be used to solve non-uniform gratings. This method is effective in the analysis of the almost-periodic grating. A non-uniform fiber Bragg grating can be divided into many uniform sections along the fiber. The incident light wave propagated through each uniform section i can be described by a transfer matrix F_i. For the structure of the fiber Bragg grating, the matrix F_i can be written as [37].

$$F_i = \begin{bmatrix} \cosh(\gamma_B\Delta z) - i\dfrac{\hat{\sigma}}{\gamma_B}\sinh(\gamma_B\Delta n(z)) & -i\dfrac{k}{\gamma_B}\sinh(\gamma_B\Delta z) \\ i\dfrac{k}{\gamma_B}\sinh(\gamma_B\Delta z) & \cosh(\gamma_B\Delta z) + i\dfrac{\hat{\sigma}}{\gamma_B}\sinh(\gamma_B\Delta n(z)) \end{bmatrix}, \tag{8}$$

where γ_B is denoted as

$$\gamma_B = \sqrt{k^2 - \hat{\sigma}^2}. \tag{9}$$

The whole grating can be represented in matrix form as

$$\begin{bmatrix} R(L) \\ S(L) \end{bmatrix} = F_M F_{M-1} \cdots F_i \cdots F_1 \begin{bmatrix} R(0) \\ S(0) \end{bmatrix}, \tag{10}$$

where L is the length of the medium. The amplitude of the reflection coefficient can be written as

$$\rho = \frac{S(0)}{R(0)}. \tag{11}$$

3. GENETIC ALGORITHM AND INVERSE PROBLEM

A genetic algorithm [39, 40] belongs to a class of evolutionary computation techniques [41–43] based on models of biological evolution. These methods have proved useful in domains that are not well understood or for search spaces, which are too large to be efficiently searched by standard methods. The GAs paradigm uses selection and recombination in various formulations to sample the search space. Solutions based on GAs approach to the problems are coded to mimic the genetic make up of biological organisms. Each individual in the population represents a possible solution to the problem. A fitness value, derived from the problem's objective function is assigned to each member of the population. Individuals that represent better solutions are awarded higher fitness values, thus enabling them to survive more generations. The GAs searches for better solutions by letting the fitter individuals take over the population through a combined stochastic process of selection and recombination. Although the main operators that influence the GAs performance are only three (i.e., selection, crossover and mutation) and their interaction is highly complex and slight variations in their implementations results in a variety of models. The different models depend on factors such as:

1. Selection method and mechanism,
2. Parent replacement method,
3. Crossover and mutation method,
4. Serial or parallel implementation,
5. Type of problem to be solved, whether a unimodal or multimodal objective function is expected.

The GAs model to be used is chosen after a careful analysis of the problem to be solved.

A standard genetic algorithm scheme is shown in Fig. 1. Operation of the method is as follows.

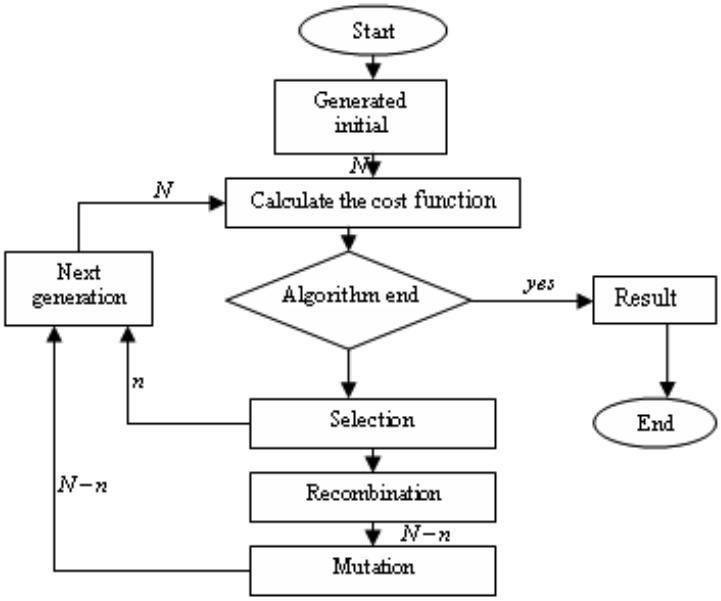

Figure 1. General scheme of the genetic algorithm.

In this method it is assumed that N is the number of first generation (individuals). Also, in the selection part, between all individuals in the current population are chose those, who will continue and by means of crossover and mutation will produce offspring population. At this stage the best n individuals are directly transferred to the next generation. The theoretical basis of the genetic algorithm and the role of its various operators are well treated in [39, 40, 44]. The application of this algorithm to the reconstruction of Fiber Bragg Gratings is described in the following.

In our approach, the GAs is used to discriminate the kind of Apodization and Chirped functions. After discriminating each function, the GAs algorithm search to calculate the parameters of the identified grating. In this paper, five mediums are considered and a GAs based method is applied to discriminate among them.

In the first stage and second stage of the proposed methodology, the following scheme is used for discrimination and identification.

This new methodology is elaborated more precisely below and the function of each block in the Fig. 2 is investigated.

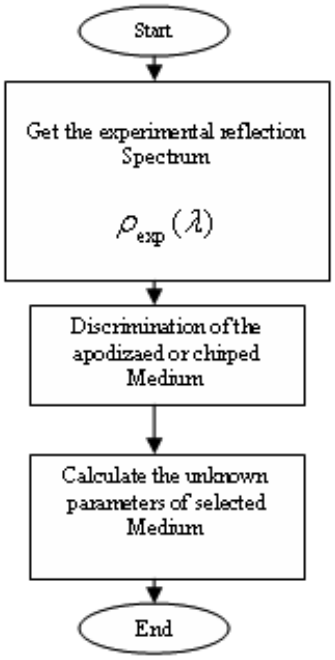

Figure 2. The scheme of inverse scattering with GA.

a) Experimental Reflection Spectrum- In our case instead of the reflection spectrum, we simulated the coupled wave equations using Transfer Matrix Method (TMM) and inserted into GAs algorithm.

b) Discrimination of the Medium- For explaining the operation of this block Fig. 3 should be considered. There is different GAs blocks (all possibilities) associated with each medium and denoted in presented block diagram as $GA_1, \ldots, GA_q$, where q is the total number of type of the considered mediums. Then the GAs search to minimize the fitness function for each medium illustrated in the block diagram respectively. After running a few iterations of GAs for each block (medium), a vector including error between the experimental values and the calculated ones is computed. The number of iterations is so important in this case for precise determination of type of the medium. In otherwise the GAs will find wrong medium type. In this work two iterations for simulation are considered. We expect that the corresponding medium to the given reflection spectrum has the

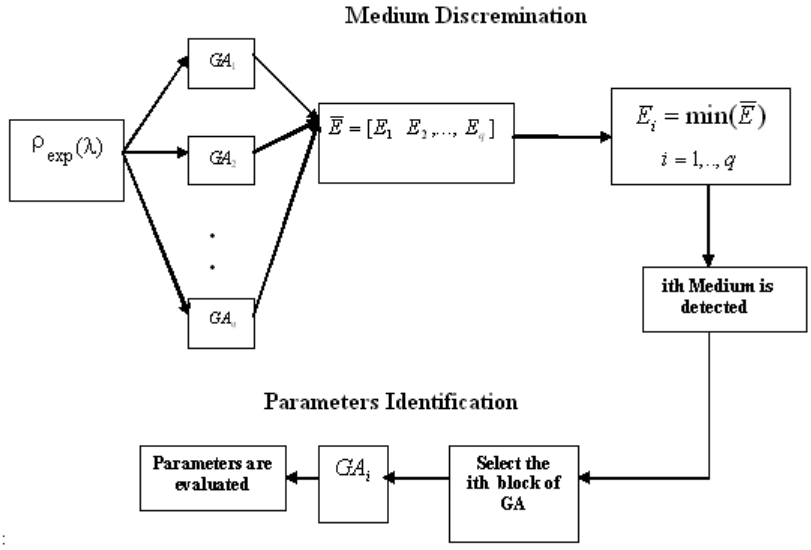

Figure 3. The scheme of discriminator and identification blocks with GAS.

minimum value in this vector. So, using the obtained error vector, the minimum value corresponds to the type of suitable medium for identification and approximation. The measured reflection coefficient should be sampled precisely to obtain high resolution and more difference between computed errors for different blocks and type of mediums.

c) Identification of the Medium parameters- After discriminating the parameters of identified medium can be evaluated. To do that the measured reflection coefficient is considered as the input for the GAs block. Then the GAs searches to minimize the fitness function to obtain the parameters of the medium. In this case we considered 50 iterations for optimization.

d) The GA blocks- The GA blocks in this algorithm for both discrimination and identification are the same. In this section, we describe in details these blocks as follows. This procedure consists of several steps as presented in Fig. 4.

1. The trial values for medium parameters according to physical limitations are chosen.
2. The reflection coefficient for the proposed parameters in first step

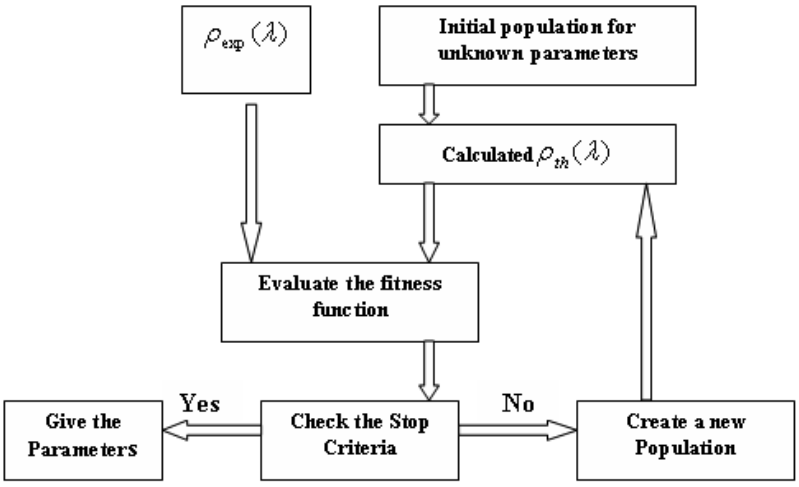

Figure 4. The scheme showing the GAS block (steps of optimization).

is calculated by using the transfer matrix method ($\rho_{th}(\lambda)$).

3. By use of the computed reflection spectrum in second step ($\rho_{th}(\lambda)$), the bandwidth and maximum reflection coefficient ($BW_{th}(\lambda), \rho_{th\,\max}(\lambda)$) can be extracted. These extracted parameters and similar cases from experimental data are used to make the fitness function (Eq. (13)).
4. For all of the initial population the fitness function is evaluated and then according to GAs operators (selection, crossover and mutation) for minimizing the fitness function, the next population is formatted and after that the next iteration is generated. The GAs run until the required criterion is eventually fulfilled.

After applying the mentioned above algorithm, the unknown medium parameters can be obtained.

e) Initial Population- The initial population for each block of GAs depends on the necessary unknown parameters of the medium according to physical model for the complex Bragg gratings.

Therefore we consider a $N_p \times M$ matrix as follows.

$$\overline{U} = [\overline{u}_1 \;\; \overline{u}_2 \;\; \cdots \;\; \overline{u}_m]_{N_p \times M}\,, \tag{12}$$

where N_p and M denote the number of population for each variable and the number of variables respectively. In this paper, we consider $N_p = 50$.

f) Fitness Function- The choice of the fitness function is fundamental in order that a correct and efficient search of the solution is carried out by the algorithm. In our problem the fitness is a function that measures the distance between the theoretical and the experimental reflection coefficient, bandwidth, and the maximum reflection, which should be minimized. In this paper the fitness function is proposed to be as

$$E = \sum_{j}^{n_s} |\rho_{\exp}(\lambda_j) - \rho_{th}(\lambda_j)| + |BW_{\exp}(\lambda) - BW_{th}(\lambda)| + |\rho_{\exp}(\lambda) - \rho_{th}(\lambda)| \tag{13}$$

where λ_j and n_s are the sampled wavelengths of the reflection coefficient and the number of samples respectively.

g) Operators- In this section we consider three most important operators as

1. Selection- Selection options specify how the genetic algorithms choose parents for the next generation. We choose this function stochastically uniform. The selection function, stochastic uniform, lays out a line in which each parent corresponds to a section of the line of length proportional to its scaled value. The algorithm moves along the line in steps of equal size. At each step, the algorithm allocates a parent from the section it lands on. The first step is a uniform random number less than the step size.

2. Crossover- Crossover options specify how the genetic algorithm combines two individuals, or parents, to form a crossover child for the next generation. Crossover function specifies the function that performs the crossover. We used the two point function for crossover. Two-point function selects two random integer m and n between 1 and Number of variables.

The function selects

- Vector entries numbered less than or equal to m from the first parent.
- Vector entries numbered from m+1 to n, inclusive, from the second parent.
- Vector entries numbered greater than n from the first parent.

The algorithm then concatenates these genes to form a single gene. For example, if p_1 and p_2 are the parents $p_1 = [a\ b\ c\ d\ e\ f\ g\ h]$, $p_2 =$ [1 2 3 4 5 6 7 8] and the crossover points are 3 and 6, the function returns the following child.

$$\text{Child} = [a\ b\ c\ 4\ 5\ 6\ g\ h].$$

3. Mutation- Mutation options specify how the genetic algorithm makes small random changes in the individuals in the population to create mutation children. Mutation provides genetic diversity and enables the genetic algorithm to search a broader space. We choose the Gaussian function as the mutation operator.

4. SIMULATION RESULTS AND DISCUSSION

In this section several examples are used to demonstrate the previously described algorithm. For simulation we consider five mediums.

1- Gaussian apodization profile
2- Rise-cosine apodization profile
3- Sinc apodization profile
4- Linear chirped profile
5- Gaussian apodization and linear chirped profile

After discrimination of the medium by first part of the proposed approach, the algorithm starts to identify the unknown parameters. For uniform FBG the following values are considered.

1. The length of grating $(L) = 10\,\text{mm}$,
2. The period of grating $(\Lambda) = 0.5356\,\mu\text{m}$,
3. The effective refractive index $(n_{eff}) = 1.447$.

For the all of histogram figures (Current best individual versus number of variables), the parameters are normalized as follows.

For example, $\delta n(z) = 8 \times 10^{-4}$ and $\alpha = 0.5 \times L$ are shown with only 8 and 5 respectively.

4.1. Gaussian Apodization Profile

In this case the Gaussian profile for apodization $(g(z))$ is considered. So, the modulation depth of the index of refraction $(\Delta n(z))$ is as follows.

$$\Delta n(z) = \delta n(z) \exp\left[-20\left(\frac{z - 0.5L}{\alpha}\right)\right] \tag{14}$$

For this Apodization the amplitude of the index modulation $(\delta n(z))$ and the Gaussian parameter (α) are important and affect the FBG characteristics strongly. Fig. 5 shows effect of the parameters on the reflection coefficient and apodization profile respectively. For illustration of these effects three following cases are considered.

1- $\delta n(z) = 8 \times 10^{-4},\ \alpha = 0.5 \times L$ (Solid line)

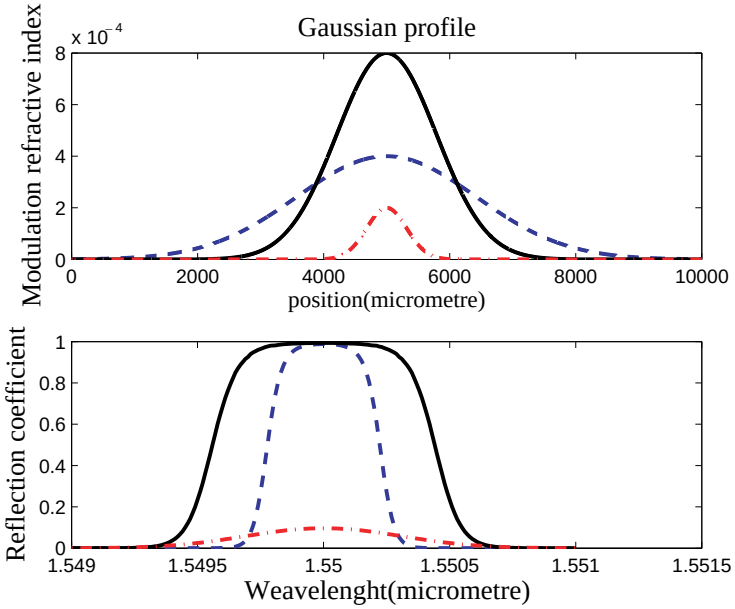

Figure 5. The modulation depth of the refractive index and the corresponding reflection coefficient for three considered cases.

2- $\delta n(z) = 4 \times 10^{-4},\ \alpha = 0.9 \times L$ (Dash line)
3- $\delta n(z) = 2 \times 10^{-4},\ \alpha = 0.2 \times L$ (Dash-dot line)

For this case the initial population for individuals considered as

$$\overline{U} = \left[\overline{\delta} n(z) \quad \overline{\alpha}\right]_{50\times 2} \tag{15}$$

The measured reflection coefficient for Gaussian apodization corresponds to the full numerical simulation for $\alpha = 0.5 \times L$, $\delta n(z) = 8 \times 10^{-4}$, and the reconstructed medium parameters using our proposed approach are $\alpha = 0.499666 \times L$ and $\delta n(z) = 7.99885 \times 10^{-4}$. As it is shown the reconstructed values are so close to input measured values.

Fig. 6 shows the evaluated fitness function in each generation as well as the calculated parameters.

To illustrate the ability of the reconstruction of the medium, we show the coupling coefficient of the medium in both real and reconstructed parameters in Fig. 7. As it is illustrated the curve corresponding to the real parameters (solid line) and reconstructed parameters (dot line) are so close together and this shows the ability of the proposed approach.

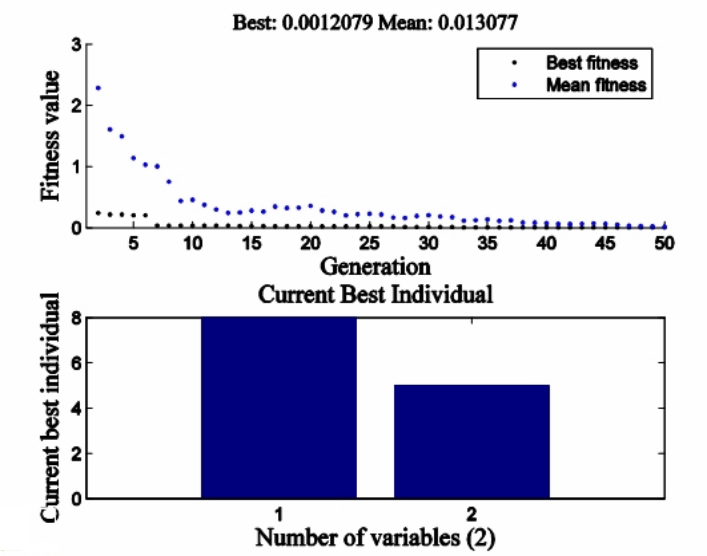

Figure 6. The evaluated fitness function and the calculated parameters.

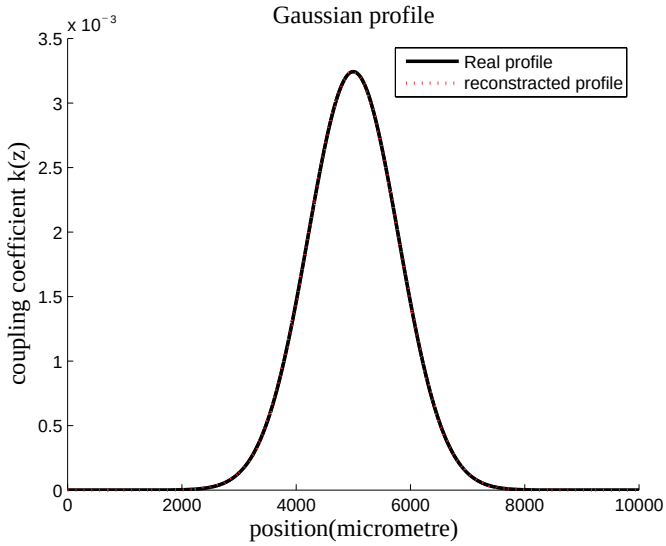

Figure 7. The coupling coefficient for real parameters (solid lines) and reconstructed ones (dot lines).

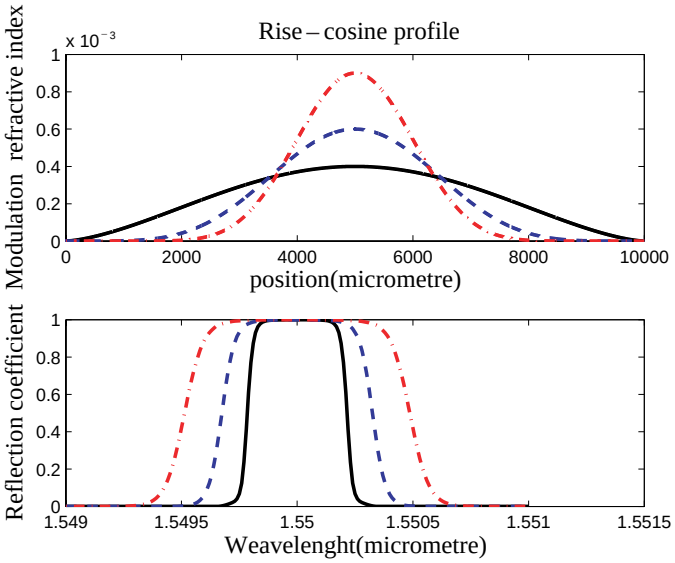

Figure 8. The modulation depth of the refractive index and the corresponding reflection coefficient for three considered cases.

4.2. Rise-Cosine Apodization Profile

In this case the Rise-Cosine profile for apodization ($g(z)$) is considered. So, the modulation depth of the index of refraction ($\Delta n(z)$) is as follows.

$$\Delta n(z) = \delta n(z) \cos^n \left(0.5\pi \left[\frac{2 \times (z - 0.5L)}{L} \right] \right) \tag{16}$$

In this apodization the amplitude of the index modulation ($\delta n(z)$) and the power degree (n) are important and affect the FBG characteristics strongly. Fig. 8 shows the effect of the parameters on the reflection coefficient and apodization profile respectively. For illustration of these effects three following cases are considered.

1- $\delta n(z) = 4 \times 10^{-4}$, $n = 1.5$ (Solid line)
2- $\delta n(z) = 6 \times 10^{-4}$, $n = 5$ (Dash line)
3- $\delta n(z) = 9 \times 10^{-4}$, $n = 10$ (Dash-dot line)

For this case the initial population for individuals considered as

$$\overline{U} = \left[\overline{\delta} n(z) \;\; \overline{n} \right]_{50 \times 2} \tag{17}$$

The measured reflection coefficient for Rise-Cosine apodization corresponds to the full numerical simulation for $n = 1.5$, $\delta n(z) =$

4×10^{-4}, and the reconstructed medium parameters using our proposed approach are $n = 1.49584$ and $\delta n(z) = 3.99949 \times 10^{-4}$. As it is shown the reconstructed values are so close to input measured values.

Fig. 9 shows the evaluated fitness function in each generation as well as the calculated parameters.

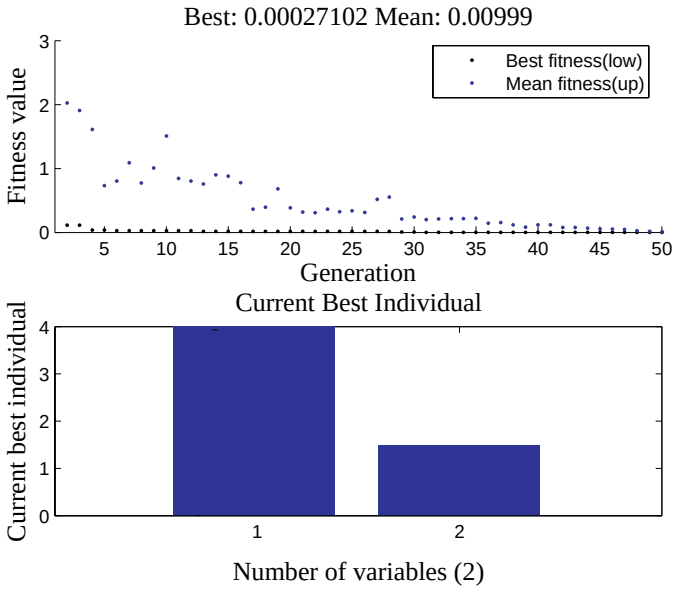

Figure 9. The evaluated fitness function and the calculated parameters.

To illustrate the ability of the reconstruction of the medium, we show the coupling coefficient of the medium in both real and reconstructed parameters in Fig. 10. As it is illustrated the curve corresponding to the real parameters (solid line) and reconstructed parameters (dot line) are so close together and this shows the ability of the proposed approach.

4.3. Sinc Apodization Profile

In this case the Sinc profile for apodization ($g(z)$) is considered. So, the modulation depth of the index of refraction ($\Delta n(z)$) is as follows.

$$\Delta n(z) = \delta n(z) \sin c^n \left(2\pi \left[\frac{(z - 0.5L)}{L}\right]\right) \tag{18}$$

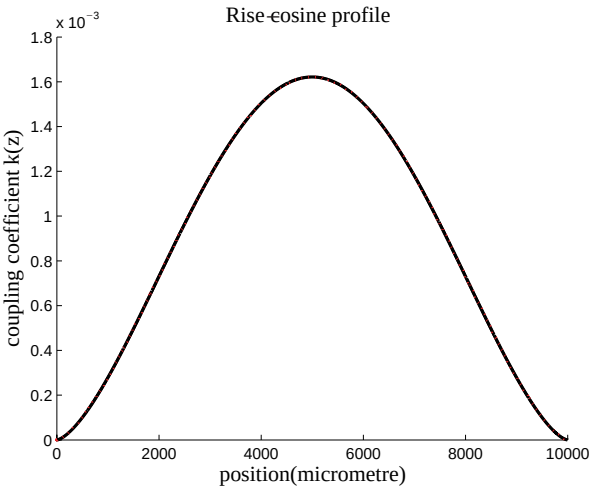

Figure 10. The coupling coefficient for real parameters (solid lines) and reconstructed ones (dot lines).

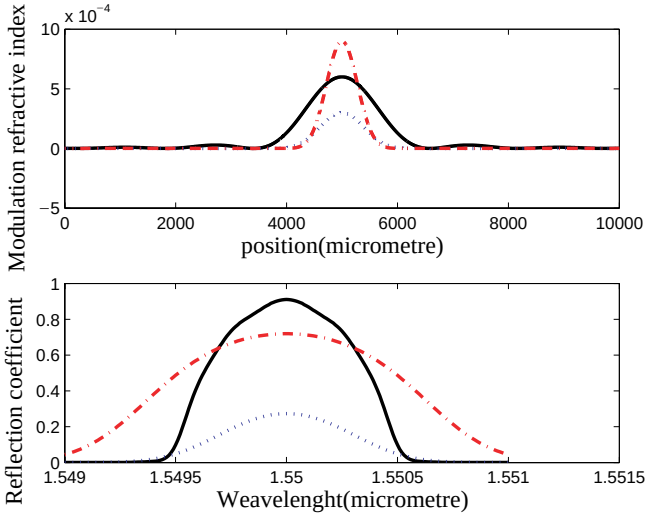

Figure 11. The modulation depth of the refractive index and the corresponding reflection coefficient for three considered cases.

In this apodization the amplitude of the index modulation ($\delta n(z)$) and the power degree (n) are important and affect the FBG characteristics strongly. Fig. 11 shows the effect of the parameters on the reflection

coefficient and apodization profile respectively. For illustration of these effects three following cases are considered.

1- $\delta n(z) = 6 \times 10^{-4},\ n = 2$ (Solid line)
2- $\delta n(z) = 3 \times 10^{-4},\ n = 5$ (Dash line)
3- $\delta n(z) = 9 \times 10^{-4},\ n = 10$ (Dash-dot line)

For this case the initial population for individuals considered as

$$\overline{U} = \left[\overline{\delta} n(z) \ \ \overline{n}\right]_{50\times 2} \tag{19}$$

The measured reflection coefficient for Sinc Apodization corresponds to the full numerical simulation for $n = 2,\ \delta n(z) = 6 \times 10^{-4}$, and the reconstructed medium parameters using our proposed approach are $n = 2.00259$ and $\delta n(z) = 5.9938 \times 10^{-4}$. As it is shown the reconstructed values are so close to input measured values.

Fig. 12 shows the evaluated fitness function in each generation as well as the calculated parameters.

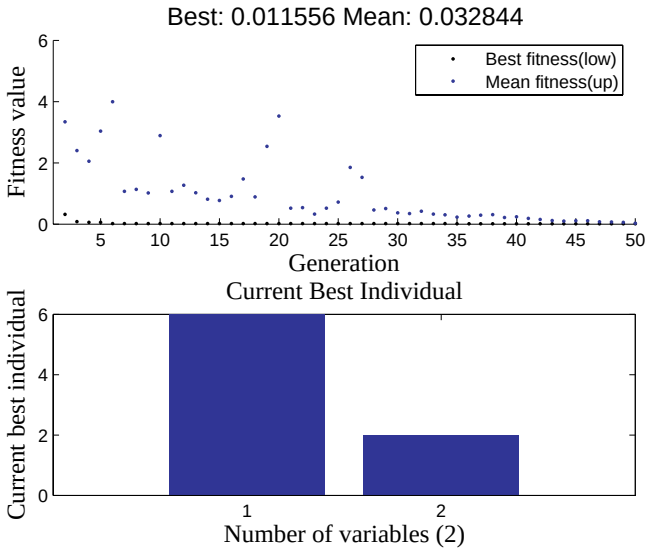

Figure 12. The evaluated fitness function and the calculated parameters.

To illustrate the ability of the reconstruction of the medium, we show the coupling coefficient of the medium in both real and reconstructed parameters in Fig. 13. As it is illustrated the curve corresponding to the real parameters (solid line) and reconstructed

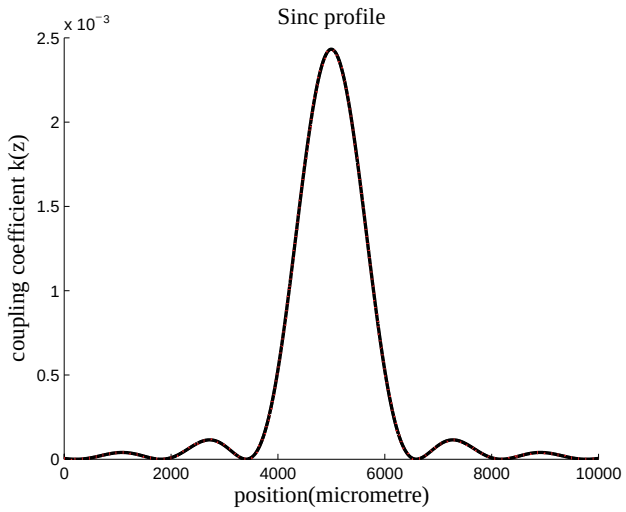

Figure 13. The coupling coefficient for real parameters (solid lines) and reconstructed ones (dot lines).

parameters (dot line) are so close together and this shows the ability of the proposed approach.

4.4. Linear Chirp Profile

In this case linear chirped is considered. According to linear chirp function the following relation is defined [28].

$$\frac{1}{2}\frac{d\Phi}{dz} = F\frac{z}{L^2}, \tag{20}$$

where F is the chirp parameter and defined as

$$F = \frac{L^2}{z^2}\Phi(z) = -4\pi n_{eff}\frac{L^2}{\lambda_D^2}\frac{d\lambda_D}{dz}, \tag{21}$$

where $\frac{d\lambda_D}{dz}$ is the rate of the chirp in the complex Bragg grating.

1- $\delta n(z) = 8 \times 10^{-4}$, $\frac{d\lambda_D}{dz} = 3 \times 10^{-7}$ (Solid line)

2- $\delta n(z) = 2 \times 10^{-4}$, $\frac{d\lambda_D}{dz} = 2 \times 10^{-7}$ (Dash line)

3- $\delta n(z) = 4 \times 10^{-4}$, $\frac{d\lambda_D}{dz} = 4 \times 10^{-7}$ (Dash-dot line)

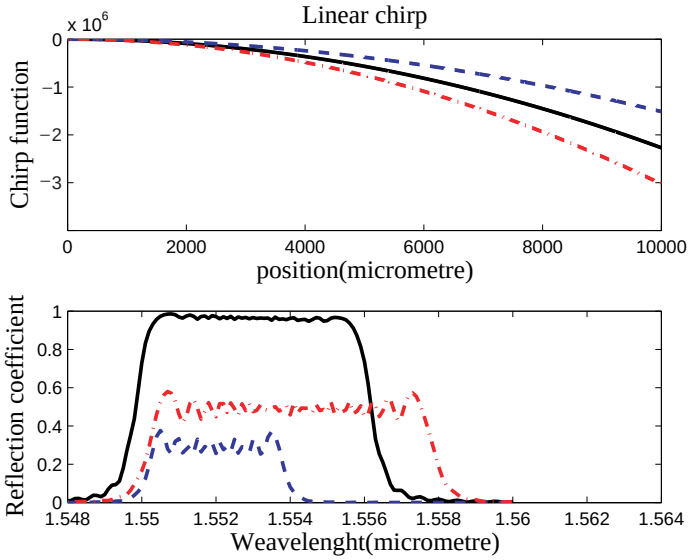

Figure 14. The Chirp function and the corresponding reflection coefficient for three considered cases.

For this case the initial population for individuals considered as

$$\overline{U} = \left[\overline{\delta}n(z) \quad \frac{d\lambda_D}{dz}\right]_{50\times 2} \tag{22}$$

The measured reflection coefficient for Linear Chirped function corresponds to the full numerical simulation for $\frac{d\lambda_D}{dz} = 3 \times 10^{-7}$, $\delta n(z) = 8 \times 10^{-4}$, and the reconstructed medium parameters using our proposed approach are $\frac{d\lambda_D}{dz} = 2.99884 \times 10^{-7}$ and $\delta n(z) = 7.9955 \times 10^{-4}$. As it is shown the reconstructed values are so close to input measured values.

Fig. 15 shows the evaluated fitness function in each generation as well as the calculated parameters.

To illustrate the ability of the reconstruction of the medium, we show the coupling coefficient of the medium in both real and reconstructed parameters in Fig. 16. As it is illustrated the curve corresponding to the real parameters (solid Line) and reconstructed parameters (dot Line) are so close together and this shows the ability of the proposed approach.

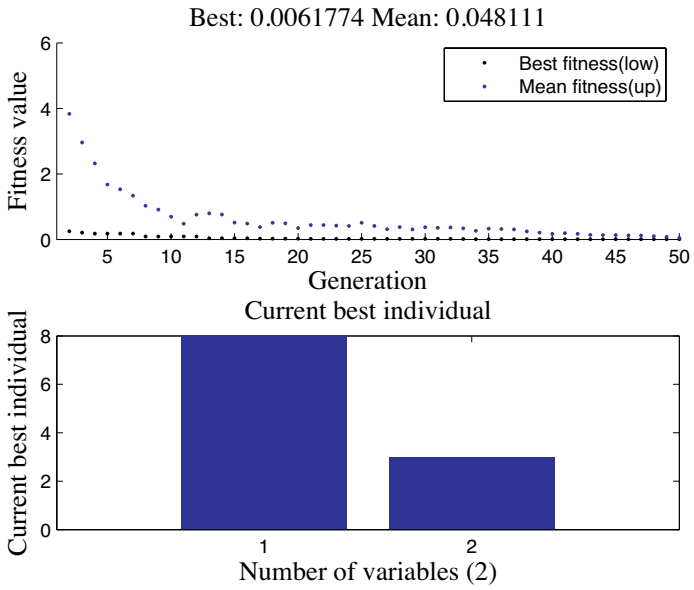

Figure 15. The evaluated fitness function and the calculated parameters.

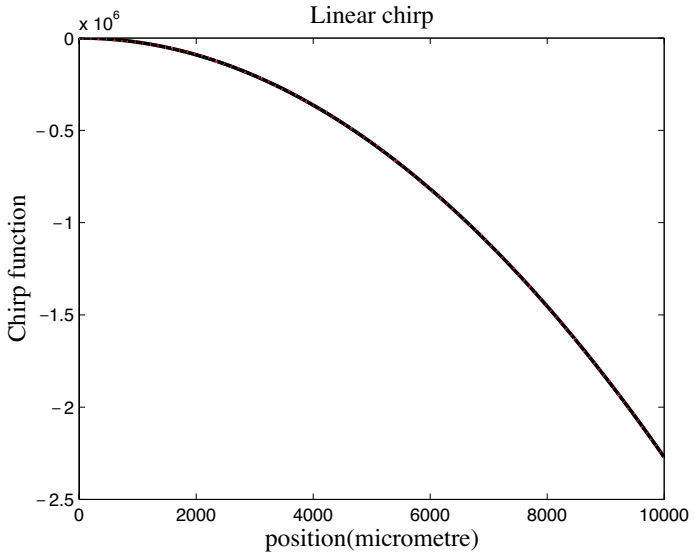

Figure 16. The Chirp function for real parameters (solid lines) and reconstructed ones (dot lines).

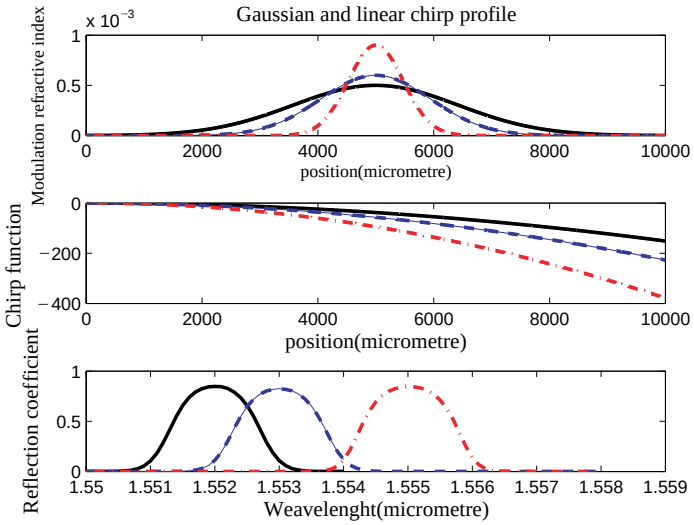

Figure 17. The coupling coefficient, Chirp function and the reflection coefficient.

4.5. Gaussian Apodization and Linear Chirped Profile

In this case, we consider simultaneously the Gaussian Apodization and Linear chirp function for investigating. For this case the following data are used.

1- $\delta n(z) = 5 \times 10^{-4},\ \frac{d\lambda_D}{dz} = 2 \times 10^{-7},\ \alpha = 0.9 \times L$ (Solid line)

2- $\delta n(z) = 6 \times 10^{-4},\ \frac{d\lambda_D}{dz} = 3 \times 10^{-7},\ \alpha = 0.6 \times L$ (Dash line)

3- $\delta n(z) = 9 \times 10^{-4},\ \frac{d\lambda_D}{dz} = 5 \times 10^{-7},\ \alpha = 0.3 \times L$ (Dash-dot line)

For this case the initial population for individuals considered as

$$\overline{U} = \left[\overline{\delta}n(z) \quad \frac{d\lambda_D}{dz} \quad \overline{\alpha}\right]_{50\times 3} \tag{23}$$

The measured reflection coefficient for simultaneous Gaussian apodization and Linear Chirped function corresponds to the full numerical simulation for $\frac{d\lambda_D}{dz} = 2 \times 10^{-7},\ \delta n(z) = 5 \times 10^{-4},\ \alpha = 0.9 \times L$, and the reconstructed medium parameters using our proposed approach are $\frac{d\lambda_D}{dz} = 2.00013 \times 10^{-7},\ \alpha = 0.894597 \times L$ and $\delta n(z) = 4.99864 \times 10^{-4}$. As it is shown the reconstructed values are so close to input measured values.

Fig. 18 shows the evaluated fitness function in each generation as well as the calculated parameters.

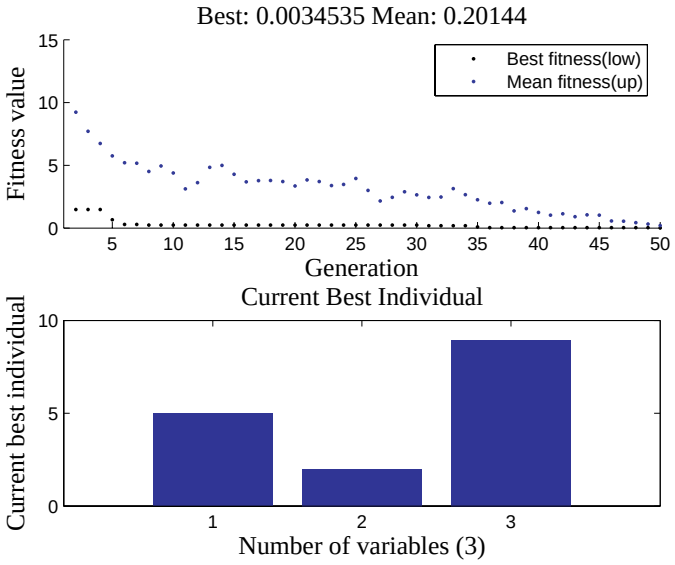

Figure 18. The evaluated fitness function and the calculated parameters.

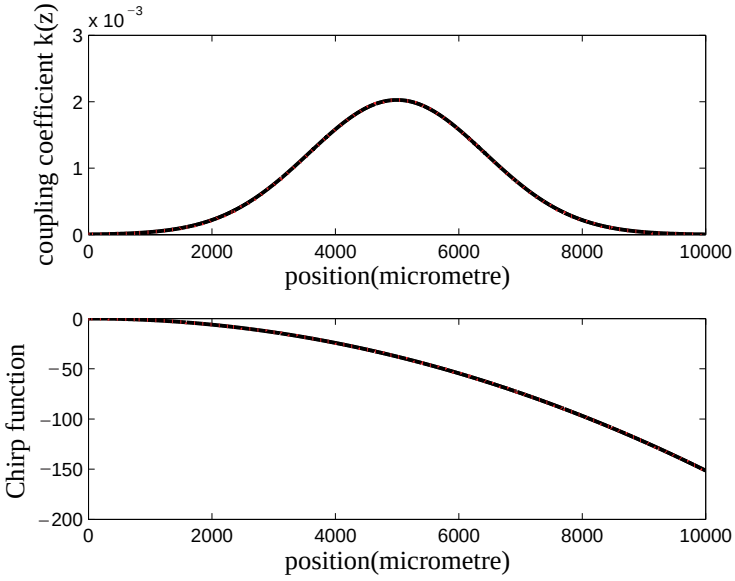

Figure 19. The coupling coefficient and Chirp function vs. position for real parameters (solid lines) and reconstructed ones (dot lines).

To illustrate the ability of the reconstruction of the medium, we show the coupling coefficient of the medium in both real and reconstructed parameters in Fig. 19. As it is illustrated the curve corresponding to the real parameters (solid line) and reconstructed parameters (dot line) are so close together and this shows the ability of the proposed approach.

5. CONCLUSION

In this paper a novel method for discrimination and identification of the complex Bragg Gratings has been developed. For this purpose the Genetic Algorithm was used. The proposed method has been applied to five interesting cases. In all cases, the presented method had good compatibility with full numerical simulations. The presented method is new and able to identify so complex mediums.

ACKNOWLEDGMENT

The authors kindly appreciate Mr. M. Savadi Oskouee and Amin Yazdanpanah-Goharrizi for their closely collaboration and their reconstructive comments. Mr. M. Savadi Oskouee is with Department of Electrical Engineering, University of Tabriz, Tabriz, Iran and Mr. Amin Yazdanpanah-Goharrizi is with Department of Electrical Engineering, K. N. Toosi University of Technology, Tehran, Iran.

REFERENCES

1. Matsuhara, M., K. O. Hill, and A. Watanabe, "Optical-waveguide filters: Synthesis," *J. Opt. Soc. Am.*, Vol. 65, 804–809, 1975.
2. Peral, E., J. Capmany, and J. Marti, "Iterative solution to the Gel'fand-Levitan-Marchenko coupled equations and applications to synthesis of fiber gratings," *IEEE J. Quantum Electron.*, Vol. 32, 2078–2084, 1996.
3. Feced, R., M. N. Zzervas, and M. A. Muriel, "An efficient inverse scattering algorithm for the design of non uniform fiber Bragg gratings," *IEEE J. Quantum Electronics*, Vol. 35, 1105–1115, 1999.
4. Winick, K. A. and J. E. Roman, "Design of corrugated waveguide filters by Fourier Transform techniques," *IEEE J. Quantum Electronics*, Vol. 26, 1918–1929, 1990.

5. Roberts, P. and G. Town, "Design of microwave filters by inverse scattering," *IEEE Transaction on Microwave Theory and Techniques*, Vol. 43, 739–743, 1995.
6. Loh, W. H., M. J. Cole, M. N. Zervas, S. Barcelos, and R. I. Laming, "Complex grating structures with uniform phase masks based on the moving fiber-scanning technique," *Opt. Lett.*, Vol. 20, No. 20, 2051–2053, Oct. 1995.
7. Asseh, A., H. Storoy, B. E. Sahlgren, S. Sandgren, and R. A. H. Stubbe, "A writing technique for long fiber Bragg gratings with complex reflectivity profiles," *J. Lightwave Technol.*, Vol. 15, 1419–1423, Aug. 1997.
8. Song, G. H. and S. Y. Shin, "Design of corrugated waveguide filters by the Gel'fand-Levitan-Marchenko inverse-scattering method," *J. Opt. Soc. Am. A.*, Vol. 2, 1905, 1985.
9. Dobrowolski, J. A. and D. Lowe, "Optical thin film synthesis program based on the use of Fourier transforms," *Appl. Opt.*, Vol. 17, No. 19, 3039–3050, Oct. 1978.
10. Bovard, B. G., "Fourier transform technique applied to quarter wave optical coatings," *Appl. Opt.*, Vol. 27, No. 15, 3062–3063, Aug. 1988.
11. Peral, E., J. Capmany, and J. Marti, "Design of fiber grating dispersion compensators using a novel iterative solution to the Gel'fand-Levitan-Marchenko coupled equations," *Electron. Lett.*, Vol. 32, No. 10, 918–919, May 1996.
12. Skaar, J., B. Sahlgren, P. Y. Fonjallaz, H. Storoy, and R. Stubbe, "High reflectivity fiber-optic bandpass filter designed by use of the iterative solution to the Gel'fand-Levitan-Marchenko equations," *Opt. Lett.*, Vol. 23, No. 12, 933–935, June 1998.
13. Frangos, P. V., D. J. Frantzeskakis, and C. N. Capsalis, "Pulse propagation in a nonlinear optical fiber of parabolic index profile by direct numerical solution of the Gel'fand-Levitan integral equations," *Proc. Inst. Elect. Eng., pt. J*, Vol. 140, No. 2, 141–149, Apr. 1993.
14. Bruckstein, A. M., B. C. Levy, and T. Kailath, "Differential methods in inverse scattering," *SIAM J. Appl. Math.*, Vol. 45, No. 2, 312–335. Apr. 1995.
15. Bruckstein, A. M. and T. Kailath, "Inverse scattering for discrete transmission-line models," *SIAM Rev.*, Vol. 29, No. 3, 359–389, Sept. 1987.
16. Bube, K. P. and R. Burridge, "The one-dimensional inverse problem of reflection seismology," *SIAM Rev.*, Vol. 25, No. 4, 497–

559, Oct. 1983.

17. Bube, K. P., "Convergence of difference methods for one-dimensional inverse problems," *IEEE Trans. Geosci. Remote Sensing*, Vol. 22, 674–682, Nov. 1984.
18. Attiya, A. M., A. A. Kishk, and A. W. Glisson, "Analysis of two-dimensional magneto-dielectric grating slab," *Progress In Electromagnetics Research*, PIER 74, 195–216, 2007.
19. Suyama, T. and Y. Okuno, "Enhancement of TM-TE mode conversion caused by excitation of surface plasmons on a metal grating and its application for refractive index measurement," *Progress In Electromagnetics Research*, PIER 72, 91–103, 2007.
20. Khalaj-Amirhosseini, M., "Equivalent circuit model for analysis of inhomogeneous gratings," *Progress In Electromagnetics Research*, PIER 69, 21–34, 2007.
21. Kusayakin, O. P., P. N. Melezhik, A. Y. Poyedinchuk, and T. Stepanovich, "Absorbing properties of a negative permittivity layer placed on a reflecting grating," *Progress In Electromagnetics Research*, PIER 64, 135–148, 2006.
22. Ohtsu, M., Y. Okuno, A. Matsushima, and T. Suyama, "A combination of up- and down-going floquet modal functions used to describe the field inside grooves of a deep grating," *Progress In Electromagnetics Research*, PIER 64, 293–316, 2006.
23. Brovenko, A., P. N. Melezhik, A. Y. Poyedinchuk, and N. P. Yashina, "Surface resonances of metal stripe grating on the plane boundary of metamaterial," *Progress In Electromagnetics Research*, PIER 63, 209–222, 2006.
24. Khalaj-Amirhosseini, M., "Scattering of inhomogeneous two-dimensional periodic dielectric gratings," *Progress In Electromagnetics Research*, PIER 60, 165–177, 2006.
25. Attiya, A. M. and A. A. Kishk, "Modal analysis of a two-dimensional dielectric grating slab excited by an obliquely incident plane wave," *Progress In Electromagnetics Research*, PIER 60, 221–243, 2006.
26. Poyedinchuk, A. Y., Y. A. Tuchkin, P. Yashinan, J. Chandezon, and G. Granet, "C-method: Several aspects of spectral theory of gratings," *Progress In Electromagnetics Research*, PIER 59, 113–149, 2006.
27. Ohki, M., K. Sato, M. Matsumoto, and S. Kozaki, "T-matrix analysis of electromagnetic wave diffraction from a dielectric coated Fourier grating," *Progress In Electromagnetics Research*, PIER 53, 91–108, 2005.

28. Skaar J. and K. Risvik, "A genetic algorithm for the inverse problem in synthesis of fiber gratings," *J. Lightwave Technol.*, Vol. 16 1928–1932, 1998.
29. Cormier, G., R. Boudreau, and S. Theriault, "Real-coded genetic algorithm for Bragg grating parameter synthesis," *J. Opt. Soc. Am. B*, Vol. 18 1771–1776, 2001.
30. Meng, Z., "Autonomous genetic algorithm for functional optimization," *Progress In Electromagnetics Research*, PIER 72, 253–268, 2007.
31. Riabi, M. L., R. Thabet, and M. Belmeguenai, "Rigorous design and efficient optimizattion of quarter-wave transformers in metallic circular waveguides using the mode-matching method and the genetic algorithm," *Progress In Electromagnetics Research*, PIER 68, 15–33, 2007.
32. Mahanti, G. K., A. Chakrabarty, and S. Das, "Phase-only and amplitude-phase only synthesis of dual-beam pattern linear antenna arrays using floating-point genetic algorithms," *Progress In Electromagnetics Research*, PIER 68, 247–259, 2007.
33. Mitilineos, S. A. and C. A. Papagianni, "Design of switched beam planar arrays using the method of genetic algorithms," *Progress In Electromagnetics Research*, PIER 46, 105–126, 2004.
34. Rodriguez, J. A., F. Ares, H. Palacios, and J. Vassal'lo, "Finding defective elements in planar arrays using genetic algorithms," *Progress In Electromagnetics Research*, PIER 29, 25–37, 2000.
35. Othonos, A. and K. Kalli, *Fibre Bragg Gratings: Fundamentals and applications in telecommunications and sensing*, Artech House, 1999.
36. Snyder, A. W. and J. D. Love, *Optical Waveguide Theory*, 542, Chapman and Hall, London, 1983.
37. Erdogan, T., "Fibre grating spectra," *Journal of Lightwave Technology*, Vol. 15, No. 8, 1277–1294, 1997.
38. Chen, L. R., S. D. Benjamin, P. W. E. Smith, and J. E. Sipe, "Ultrashort pulse reflection from fiber gratings: a numerical investigation," *Journal of Lightwave Technology*, Vol. 15, No. 8, 1503–1512, 1997.
39. Holland, J. H., *Adaptation in Natural and Artificial Systems*, 2nd edition, MIT, Cambridge, MA, 1992.
40. Goldberg, D. E., *Genetic Algorithms in Search, Optimization and Machine Learning*, Addison-Wesley, Reading, 1989.
41. Spears, W. M., K. A. De Jong, T. Baeck, and P. Bradzil, "An overview of evolutionary computation," *Proceedings of European*

Conference on Machine Learning, Vol. 667, 442–459, Springer-Verlag, Berlin, 1993.

42. Baeck, T., F. Hoffmeister, and H. P. Schwefel, "An overview of evolutionarv algorithms for parameter optimization," *J. Evol. Comput.*, K. Dejong (ed.), Vol. 1, 1–24, MIT Press, Cambridge, MA, 1993.
43. Koza, J. R., *Genetic Programming: On the programming of computers by means of natural selection*, MIT, Cambridge, 1992.
44. Horn, J., R. Belew, and L. Booker, "Finite Markov chain analysis of a genetic algorithm with niching," *Proceedings of the 4th International Conference on Genetic Algorithms*, 110–117, MorGAsn Kauffman, San Mateo, CA, 1993.